

Fixed-Bed System for Adsorption of Anionic Acid Dyes from Binary Solution onto Quaternized Kenaf Core Fiber

Intidhar Jabir Idan,^{a,b,*} Luqman Chuah Abdullah,^a Siti Nurul Ain Binti Md. Jamil,^c Maytham Kadhim Obaid,^{a,b} and Thomas Shean Yaw Choong^a

Water pollution due to the effluents from textile industries causes serious concern around the world. During the coloration process, the excess synthetic dyes are discharged into the wastewater stream. In the present research, kenaf core fiber (KCF) residue was chemically modified with (3-chloro-2-hydroxypropyl) trimethylammonium chloride (CHPTAC) to alter the surface properties and increase the surface area to develop more active sites that capture anionic dyes from aqueous solution. Fixed-bed adsorption studies were conducted to investigate the performance of using quaternized kenaf core fiber (QKCF) as an adsorbent for the removal of anionic acid dyes from a binary system. The effects of operational parameters, including inlet dye concentration, flow rate, and bed height, were studied in a fixed-bed column system, while other process parameters were fixed, *i.e.* pH and temperature at 7.5 and 27 °C, respectively. The fixed-bed column performed better with lower influent dye concentration, less flow rate of the influent, and a higher adsorbent bed depth. Overall, the present study showed that QKCF is a potential adsorbent for anionic dye removal from aqueous solutions in a fixed-bed column system.

Keywords: Binary system; Fixed-bed; Kenaf core fiber; Acid blue dye; Acid green dye; Quaternization

Contact information: a: Department of Chemical and Environmental Engineering, University Putra Malaysia, 43400 UPM Serdang, Selangor, Malaysia; b: Department of Environmental Engineering, Faculty of Engineering, University of Babylon, Babylon, Iraq; c: Department of Chemistry, Faculty of Science, University Putra Malaysia, 43400 UPM Serdang, Selangor, Malaysia;

* Corresponding author: immb2010@yahoo.com

INTRODUCTION

The most challenging mission in wastewater treatment plants is the removal of anionic dyes because they are water-soluble and produce colors that shine brightly in the water. Even very small quantities of these dyes in aqueous environments can significantly affect the transparency and quality of bodies of water, leading to water pollution. Chemical dyes absorb and reflect sunlight that enters the water, and the absorption of light decreases algal photosynthesis and can disrupt the food chain (Indrani *et al.* 2016; Pirsahab *et al.* 2016).

It is necessary to carefully monitor all effluents that are discharged from industries that carry dyes and pigments to natural water bodies and to remove the colored constituents in order to protect the aquatic environment and to also safeguard human well-being. A great number of new technologies for effluent management are being developed in response to the economic, environmental, and societal limitations that are increasingly posed by conventional wastewater systems (Mondal 2008; Shahmoradi *et al.* 2013; Shivaraju *et al.* 2017). Adsorption can remove or reduce different kinds of pollutants (*i.e.*, dyes) and is widely used in wastewater treatment plants (Hamdaoui

2006).

Recently, interest in producing an adsorbent derived from renewable, abundant, low-cost substances and generated from an agricultural origin has increased (Babel and Kurniawan 2003). Compared with the production of activated carbon, which requires high energy consumption (steam or gasification processes), the chemical modification of agricultural biomass requires less energy (no gasification) to produce an adsorbent. There has been a growing trend toward the addition of surface modifiers (Shahmoradi *et al.* 2012). One such modification process is quaternization (Yavari *et al.* 2016). To date, there has been no reported research on using quaternized kenaf core fiber (QKCF) as an adsorbent for the removal of binary acid dyes from an aqueous system. Therefore, a study on the development of QKCF as a novel adsorbent in removing binary acid dyes from aqueous solutions is needed. In this research, kenaf core fiber (KCF) was chemically modified to improve the dye removal capacities for a fixed-bed absorption system.

EXPERIMENTAL

Preparation Adsorbent from Kenaf Core Fibers

Kenaf core fiber (KCF) was selected as the raw material for the preparation of adsorbent and was collected from the Institute of Tropical Forestry and Forest Products (INTROP) in Universiti Putra Malaysia. KCF coarse powder was washed thoroughly in water to get rid of dust and undesirable particles. The collected sample of KCF was then rinsed with distilled water and oven-dried for 24 h at 50 °C to remove all moisture. The dried KCF coarse powder was sieved using stainless steel sieves to collect particle sizes from 0.25 mm to 1 mm. A specific amount of KCF (30 g) was mercerized by soaking it in a solution of 20 wt.% NaOH (62.5 g NaOH dissolved in 250 mL of distilled water) for 24 h. The basic medium swelled the fiber walls and opened the pores to improve the KCF absorbency. Mercerized kenaf core fiber (MKCF) was washed with distilled water and oven-dried at 50 °C for 24 h.

The quaternization was accomplished by reacting each gram of dried MKCF with a solution that consisted of 1.5 g of NaOH, 6.67 mL of 3-chloro-2-hydroxypropyl trimethylammonium chloride (CHPTAC) solution (with 60 wt.% in water), and 2.5 mL of distilled water. The mixture was kept in a closed container at room temperature for 24 h. The quaternized kenaf core fiber (QKCF) was washed with 0.1% acetic acid solution to halt the reaction and rinsed with distilled water until a neutral pH was attained. The QKCF was dried at 50 °C for 24 h and stored in a closed container (Idan *et al.* 2017).

Scanning electron microscopy (SEM; Hitachi Model S-3400N, Tokyo, Japan) was used to investigate the morphology of natural kenaf core fiber (NKCF) and QKCF. Samples were spread over an aluminum stub with double-sided tape and coated with a thin layer of gold. The apparatus was operated at 15 kV, and micrographs were recorded at an enlargement of 100 μm . Energy dispersive X-ray (EDX) is a surface elemental analysis used in conjunction with SEM. The instrument was operated at 20 to 30 kV.

Fourier Transform-Infrared (FT-IR) Spectrometer 100 (PerkinElmer, United Kingdom) is an essential tool to analyze surface functional groups for adsorbent materials. FTIR spectrum was used in this study to identify the characteristic functional groups in QKCF and NKCF.

Surface area, pore volume, and pore diameter of the prepared adsorbent were measured by Micromeritics 3Flex surface characterization analyzer (Norcross, GA,

USA). Nitrogen sorption isotherms were measured at 77 K. The Brunauer-Emmett-Teller (BET) method was utilized to calculate the specific surface areas. By using the non-local density functional theory (NLDFT) model, the pore volume was derived from the sorption curve. This procedure was automatically performed by software available within the instrument.

Preparation of Dyes

Acid blue 25 (AB) and Acid green 25 (AG) anionic dyes were used as adsorbates to evaluate the performance of QKCF. The structures and general properties of these two dyes are presented in Fig. 1 and Table 1, respectively.

The stock solution of a single solute of AB and AG dyes were prepared by dissolving 1.00 g of dye powder with distilled water in a volumetric flask, such that the final concentration of each single solute in the respective stock solution was 1000 mg/L. The solutions with various dye concentrations were prepared by the fresh dilution of the stock solution with distilled water prior to each adsorption study using Eq. 1,

$$C_1V_1 = C_2V_2 \quad (1)$$

where C_1 and C_2 were the required dye concentration and the stock dye concentration in mg/L, respectively, and V_1 and V_2 were the required dye volume and the stock dye volume in mL, respectively.

The ratio of mixing for each sample in binary systems was 1:1; every 100 mL of anionic dye solution was prepared by a mixture of 50 mL of AB dye and 50 mL of AG dye. The concentration of each dye was changed depending on the tests.

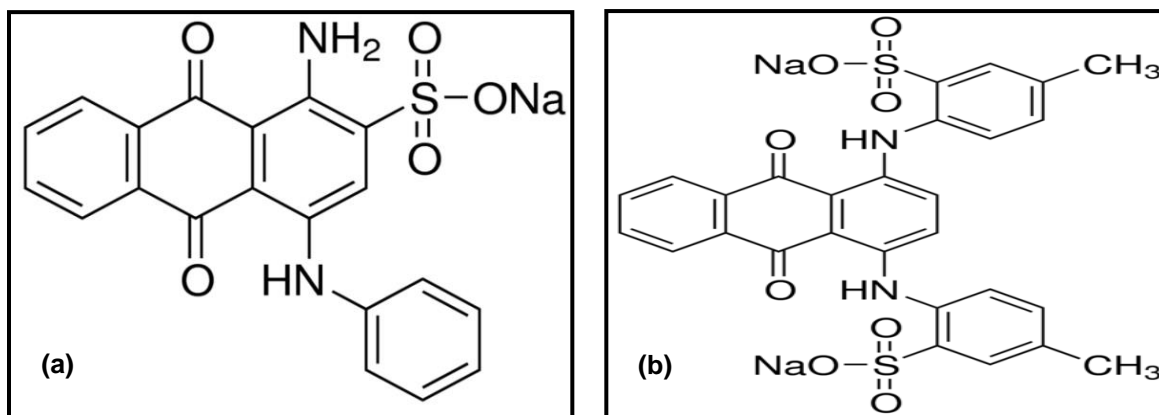


Fig. 1. Molecular structure of (a) AB dye and (b) AG dye

Table 1. General Properties of RR, RB, AB and AG Dyes

Name of Commercial Dye	λ_{\max} (nm)	Molecular Weight (g/mol)	Chemical Formula
Acid Blue 25	602	416.38	$C_{20}H_{13}N_2NaO_5S$
Acid Green 25	641	622.58	$C_{28}H_{20}N_2Na_2O_8S_2$

Fixed-bed Adsorption Studies for Binary System

Fixed-bed adsorption studies were conducted for adsorption AB and AG dyes in binary acid components on a QKCF by changing the inlet dye concentration, flow rate of

the dye inlet, and QKCF bed height.

Continuous flow adsorption studies were conducted at 27 ± 1 °C in a column made of a Pyrex glass tube that was 50 cm tall and had an inner diameter of 25 mm. A porous sintered disc was placed at the bottom of the column to prevent the loss of adsorbent, and a layer of glass wool was placed on the top of the adsorbent to prevent floating of the adsorbent. A known quantity of QKCF sorbent was packed in the column to yield the desired bed height. QKCF was soaked in deionized water for 15 min to prevent entrapped air from being held in the column. The column was washed with distilled water for 5 min at a constant flow rate before loading the dye solution.

A Watson Marlow 101U/R peristaltic pump (Watson-Marlow Limited, Falmouth, Cornwall, UK) was used to pump the dyes solution downward through the column at a chosen flow rate. The dyes solutions were placed in a tank that was connected with a pipe to the column. After a pre-determined interval of time, the outlet dyes concentration C_t (mg/L) was measured. The breakthrough curves of C_t/C_o were plotted against time.

RESULTS AND DISCUSSION

Characterization of Adsorbent

Scanning electron microscopy

The surface morphology of the NKCF and QKCF was examined using SEM (Fig. 2). The micrograph in Fig. 2a shows that the surface textures of the lignocellulosic in NKCF were rough, with uneven surfaces and some minor pores. After quaternization, the pores on the surface of the QKCF were very noticeable with distinct pore walls, as shown in Fig. 2b. They were arranged in a group of honeycombed structures. These open cylindrical and heterogeneous pores provide sites for dyes to be trapped and adsorbed on the QKCF surface (Zaini and Khairul 2014).

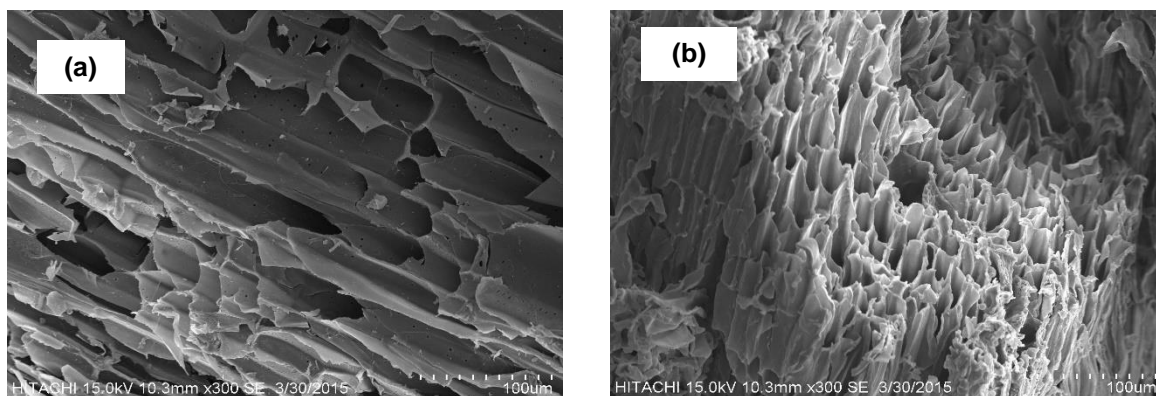


Fig. 2. SEM Micrographs of (a) NKCF and (b) QKCF

Fourier Transform Infrared Spectroscopy (FT-IR)

The FT-IR spectra of NKCF and QKCF are illustrated in Fig. 3. As can be observed from Fig. 3, the trend of the FTIR spectrum for NKCF contains some main peaks which are almost similar to many lignocellulosic plants. Some major peaks around $2950\text{-}2770\text{ cm}^{-1}$ are related to aldehyde C-H of alkane, $2517\text{-}2131\text{ cm}^{-1}$ of aromatic C=C stretching of ketone, $1732\text{-}1500\text{ cm}^{-1}$ of C=O stretching vibration of carboxylate and

1505-1059 cm^{-1} are related to medium intensity of C-N were detected. The O-H stretching vibrations at bandwidth of 3943-3 637 cm^{-1} are present in the NKCF and QKCF. The peaks located at 3263 cm^{-1} , 3569 cm^{-1} , and 3597 cm^{-1} are found on the spectrum of the QKCF; they indicate the presence of C-H, CH_2 , and free OH, respectively, whereas the peak detected at 2878 cm^{-1} on the spectrums of the QKCF represents the presence of CH_3 , CH_2 , and CH groups. Furthermore, peaks at 1655 cm^{-1} assigned to C=O stretching vibration of carboxylate, 1592 cm^{-1} for medium N-H band and 1475 cm^{-1} assigned to the NH_2 amines group is evidence of a quaternary ammonia group reacted to QKCF. The medium peak located at 1229 cm^{-1} band is assigned to the C-N medium amines. Moreover, the peaks located at 900 and 450 cm^{-1} are assigned to the =C-H and CH_2 rocking.

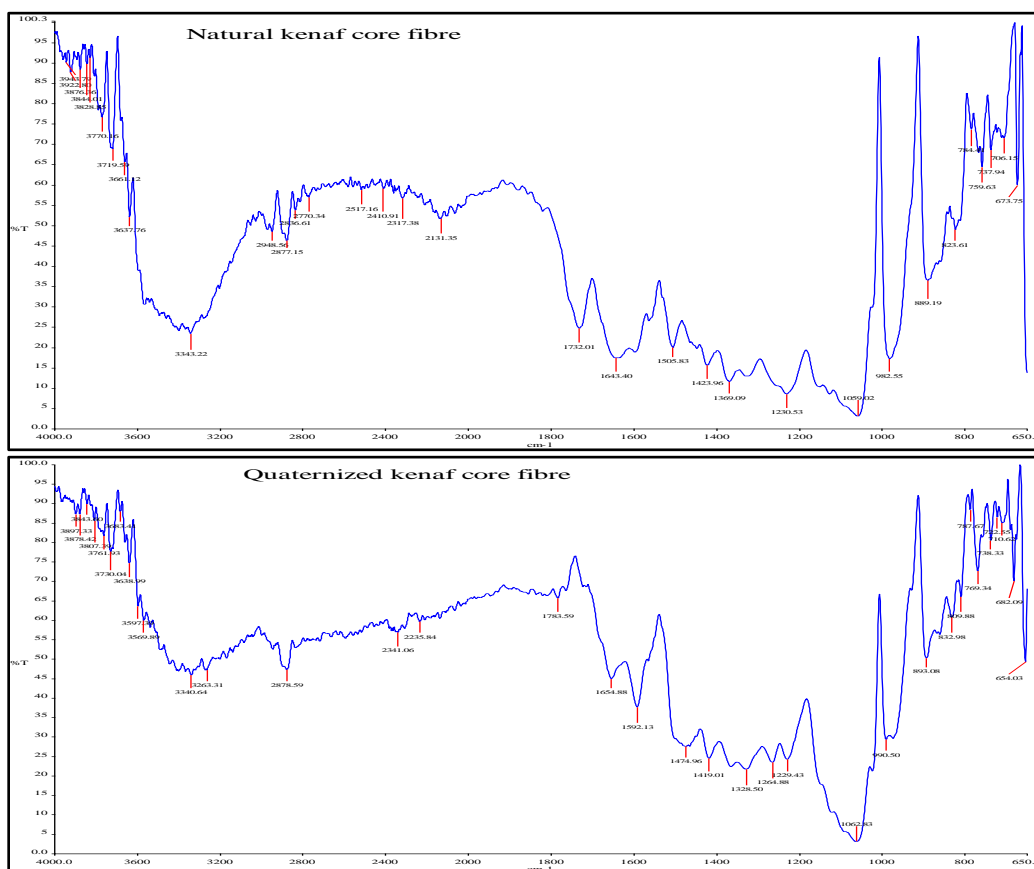


Fig. 3. FTIR spectra for natural kenaf core fiber (NKCF) and quaternized kenaf core fiber (QKCF)

BET analysis

The surface area and average pore diameter of the prepared adsorbents were determined by BET analysis. This analysis is important because a large pore removes a smaller adsorbate rapidly, but is unable to retain it permanently, which results in an overall lower removal efficiency, while a small pore would fail to capture larger adsorbates (Ahmedna *et al.* 2000). Figures 4 and 5 show the BJH plots of cumulative surface area vs. pore width and surface area plot for NKCF and QKCF, respectively. The surface area (S_{BET}) increased from 2.4 m^2/g for NKCF to 4.3 m^2/g for QKCF. The average pore diameter of NKCF was 106 nm, which indicated macropores. QKCF had an average pore diameter of 283 nm. The pore volume slightly decreased from 0.1699 cm^3/g

for NKCF to 0.1128 cm³/g for QKCF, which was attributed to the smoother texture of KCF surface after quaternization (Idan *et al.* 2017).

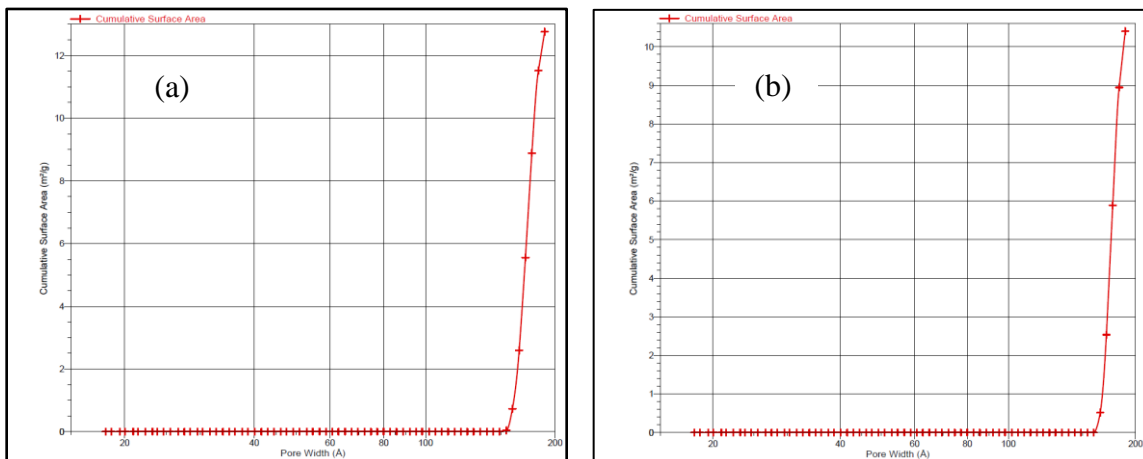


Fig. 4. BJH plots of cumulative surface area vs. pore width for (a) NKCF and (b) QKCF

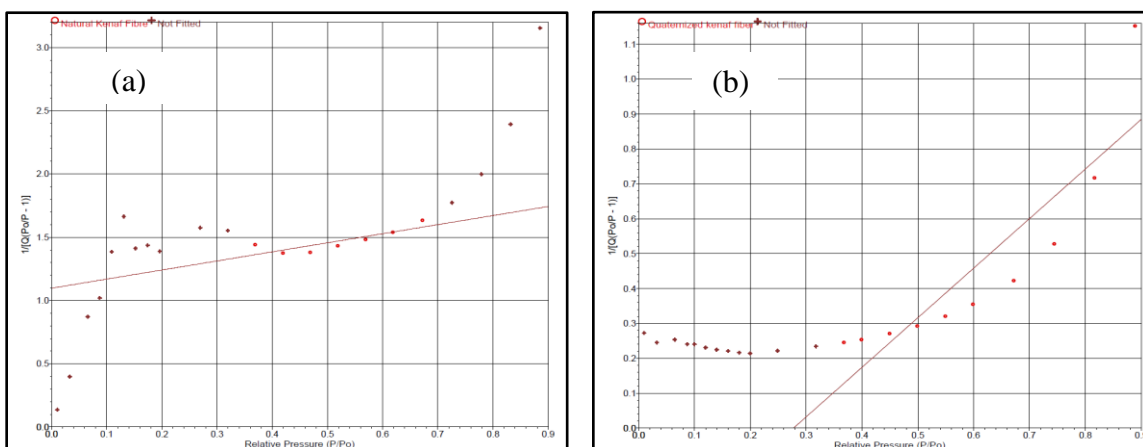


Fig. 5. BET surface area plot for (a) NKCF and (b) QKCF

Energy dispersive X-ray (EDX)

The elemental composition of carbon, oxygen, and nitrogen in the NKCF and QKCF are listed in Table 2, and the elemental percentages are shown in Fig. 6. A significant percentage of nitrogen was detected in QKCF, whereas it was not detected in NKCF. Hence, this analysis verified that the quaternary ammonia group (NH⁴⁺) reacted on QKCF and that the synthesis was successful. Moreover, the percentage of nitrogen in the QKCF sample detected by EDX was 0.88%. This result indicates that NR⁴⁺ ions were present on the QKCF surface.

Table 2. Elemental Analysis of NKCF and QKCF by EDX

Element (wt.%)	NKCF	QKCF
Carbon	39.32	41.98
Oxygen	60.68	56.66
Nitrogen	0.0	0.88

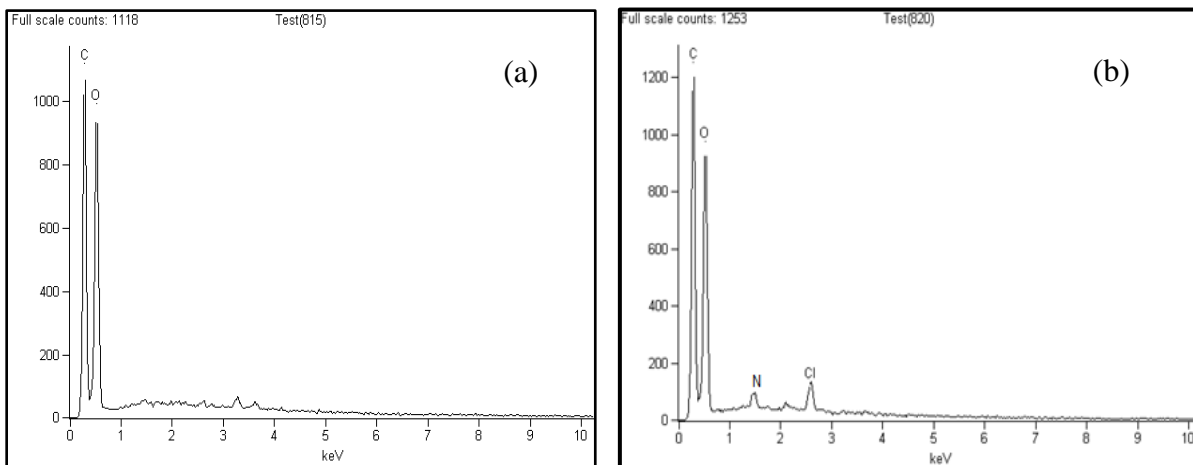


Fig. 6. EDX spectra of (a) NKCF and (b) QKCF

Measurement of Dye Concentration in Multicomponent Solution

The UV-spectrophotometer method is a common procedure for determining the dye concentration in a mixture. The linear relationship between the absorbance (A) and concentration of dye (C) (mg/L) given by the Beer-Lambert law in Eq. 2 was applied (Ekrami and Okazi 2010),

$$A = K C + E \quad (2)$$

where A is the absorbance of light at a maximum wave length (λ_{\max}), K is the absorbance coefficient (slope of linear relation), C is the concentration of dye in the solution (mg/L), and E is the intercept.

For the binary system, the total absorbance A_1 at $\lambda_{1,\max}$ (absorbance of light at maximum wave length for component 1) is the sum of absorbance in the individual components of AB and AG and can be written as Eq. 3,

$$A_1 = K_{AB1} * C_{AB} + K_{AG1} * C_{AG} \quad (3)$$

Similarly, for the total absorbance A_2 at $\lambda_{2,\max}$ (absorbance of light at maximum wave length for component 2) can be written as Eq. 4.

$$A_2 = K_{AB2} * C_{AB} + K_{AG2} * C_{AG} \quad (4)$$

The combination of the previous two equations results in Eqs. 5 and 6, respectively, which provide the values for the concentration of each dye component, C_{AB} and C_{AG} .

$$C_{AB} = \frac{(K_{AG2} * A_1) - (K_{AG1} * A_2)}{(K_{AB1} * K_{AG2}) - (K_{AB2} * K_{AG1})} \quad (5)$$

$$C_{AG} = \frac{(K_{AB1} * A_2) - (K_{AB2} * A_1)}{(K_{AB1} * K_{AG2}) - (K_{AB2} * K_{AG1})} \quad (6)$$

where K_{AB1} and K_{AG1} represent the calibration constants for dyes AB and AG at $\lambda_{1,\max}$, while K_{AB2} and K_{AG2} represent the calibration constants for dyes AB and AG at $\lambda_{2,\max}$.

To calculate the dye concentrations of each dye in the binary acid solution (AB with AG dyes), four calibration curves were built to determine four calibration coefficients using pure standard AB and AG dyes of known concentration, as illustrated in Figs. 7 and 8, which show the calibration constants for the AB and AG dyes as follows:

$K_{AB1} = 0.0267, K_{AG1} = 0.0157$ measured at $\lambda_{1,max} = 602$ nm

$K_{AB2} = 0.0246, K_{AG2} = 0.0159$ measured at $\lambda_{2,max} = 641$ nm

Thus, the concentrations of the AB and AG dyes were calculated by Eqs. 7 and 8, respectively.

$$C_{AB} = \frac{(0.0159 \times A_1) - (0.0157 \times A_2)}{(0.0267 \times 0.0159) - (0.0246 \times 0.0157)} \tag{7}$$

$$C_{AG} = \frac{(0.0267 \times A_2) - (0.0246 \times A_1)}{(0.0267 \times 0.0159) - (0.0246 \times 0.0157)} \tag{8}$$

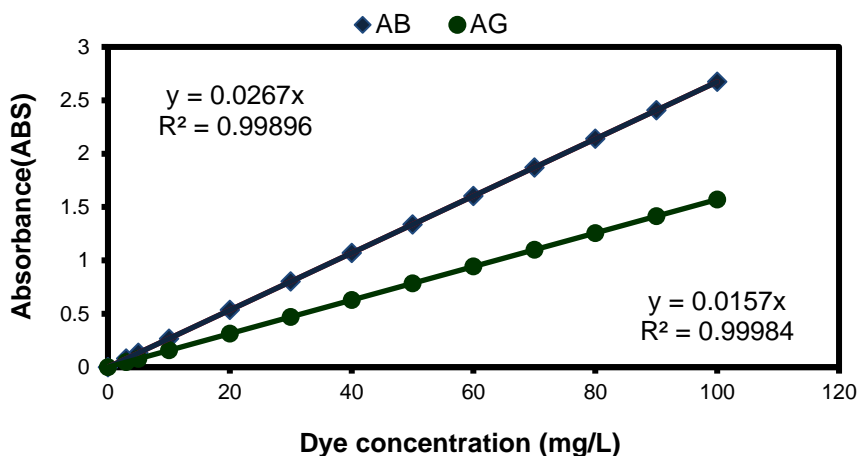


Fig. 7. Calibration curves for AB and AG dyes at $\lambda_{1,max} = 602$ nm

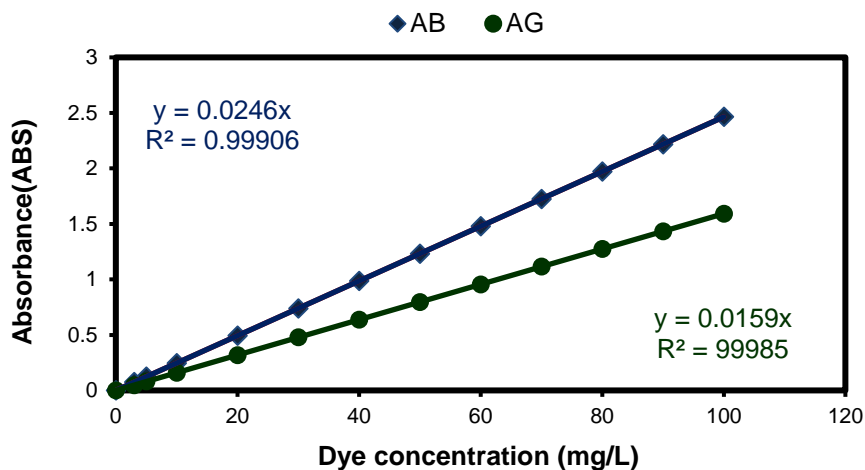


Fig. 8. Calibration curves for AB and AG dyes at $\lambda_{2,max} = 641$ nm

Fixed-Bed Adsorption Studies

In a fixed-bed sorption process, the solution enters into a continuous stream and leaves the adsorbent column. The area covered by the polluted on the inlet side is called the mass transfer zone (MTZ) and is where adsorption occurs. When the activated adsorbent material gets exhausted over a period of time, the MTZ region moves ahead and across the bed, leaving behind a region of the bed that has been saturated by contaminated substances. A breakthrough takes place when the MTZ reaches the end of

the whole bed. The breakthrough curve acts as a graphical representation of the MTZ movement across the bed. The breakthrough point occurs when the ratio of the concentration of the influent, C_o (mg/L) and the effluent, C_t (mg/L) is 0.05; the time at this point is defined as t_b (min). Generally, for industrial applications when the C_t/C_o value becomes 0.5 at time $t_{0.5}$ (min), *i.e.*, 50% breakthrough is achieved, the column adsorbent is replaced. The column adsorption capacity is estimated at this breakthrough point. Despite reaching a 50% breakthrough, the column is still operational until it reaches a value of $C_t/C_o = 0.90$, which is the column's operating limit. Furthermore, the column gets completely exhausted if the inlet and the outlet concentrations are similar *i.e.*, $C_o \approx C_t$ at time t_e . In this research, the column sorption capacity for removal acid dyes at 50% breakthrough (mg/g) was calculated by Eq. 9 (Baral *et al.* 2009).

$$\text{Column adsorption capacity at 50\% breakthrough (mg/g)} = (\text{Breakthrough time (at 50\%)} (\text{min}) \times \text{Influent flow rate (L/min)} \times \text{Inlet dye concentration (mg/L)}) / \text{mass of adsorbent in bed (g)} \quad (9)$$

Effect of inlet dyes concentration

The effect of the inlet dye concentration of the binary dyes on the column performance was studied by varying the inlet dye concentrations of 20 mg/L, 60 mg/L, and 100 mg/L for constant bed height of 6 cm and inlet flow rate of 10 mL/min. The breakthrough curves are shown in Fig. 9 for AB and AG dyes in binary acid components. The QKCF adsorbent bed was exhausted faster at the higher initial dye concentrations of AB and AG dyes in the binary systems. Table 3 shows that the breakthrough point (t_b) was reached faster with the 100 mg/L dye solution than with the other two concentrations of 20 mg/L and 60 mg/L. This phenomenon is expected with increasing influent dye concentration because the binding sites were occupied rapidly, and the QKCF adsorbent bed was saturated within a short period of time (Tan *et al.* 2008).

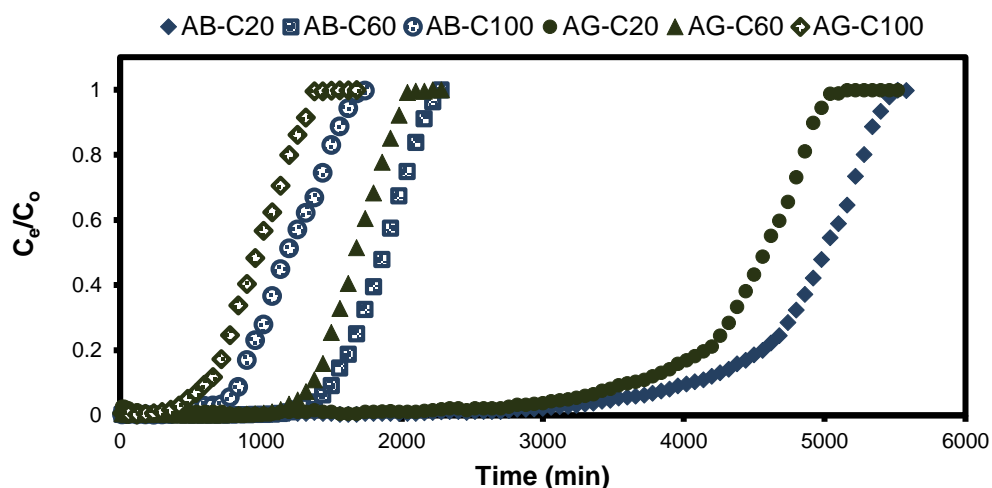


Fig. 9. Breakthrough curves for adsorption of AB and AG dyes in binary system for different initial dye concentrations (bed depth of 6 cm, flow rate of 10 mL/min, and a temperature of 27 ± 1 °C)

Effect of bed adsorbent height

Figure 10 shows the breakthrough curve obtained for the adsorption of AB and AG dyes in binary systems on QKCF for the three different bed heights of 4, 6, and 8 cm

at a constant dye concentration of 100 mg/L and an adsorbate flow rate of 10 mL/min.

A constant pattern of breakthrough curves was obtained for AB and AG dyes in binary systems over the range of bed depths studied. However, at a higher bed height, the curves tended to be flatter. In addition, Table 3 shows that both breakthrough and exhaustion times increased with an increase in the bed height from 4 cm to 8 cm. This result reflects the fact that at higher bed heights there is more mass of QKCF present in the column and more active sites to capture the dye molecules, resulting in a greater uptake capacity (Obaid *et al.* 2017). Increasing the bed depth increases the dye transfer zone. The dye transfer zone travels from the entrance side of the fixed-bed and proceeds toward the outlet side. Therefore, for the same inlet concentration, an increase in the bed height would result in a longer distance for the dye transfer zone to reach the exit of the column. Consequently, it would result with an extended breakthrough time. For higher bed depths, the increase in the QKCF mass would provide a larger service area and lead to an increase in the volume of dye solutions that need to be treated (Ahmad and Hameed 2010).

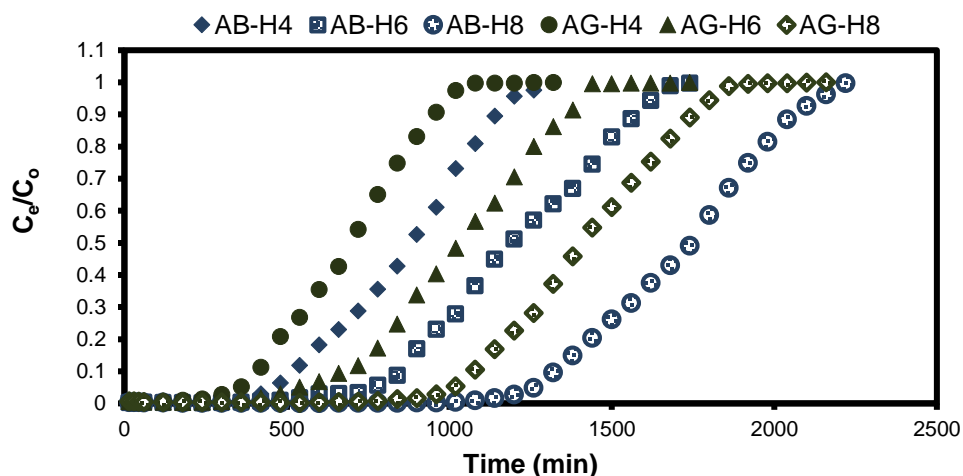


Fig. 10. Breakthrough curves for adsorption of AB and AG dyes in binary system for different bed depth (C_0 100 mg/L, flow rate 10 mL/min, temp. 27 ± 1 °C)

Effect of flow rate

The effect of inlet dyes flow rate (Q) on the adsorption of AB and AG dyes in binary system on QKCF was investigated by varying the flow rate (5 mL/min, 10 mL/min, and 15 mL/min) by keeping the inlet dye concentration constant at 100 mg/L and with a bed depth of 6 cm. The breakthrough curves are shown in Fig. 11. At a lower flow rate of 5 mL/min, a longer contact time was required, and a thin adsorption zone formed. At higher flow rate of 15 mL/min, a steeper curve and a relatively early breakthrough was observed for all the dyes.

Thus, the fixed-bed column packed with QKCF demonstrated better performance by using a lower inlet dye flow rate of 5 mL/min rather than a higher flow rate of 15 mL/min. This was due to the higher flow rate resulting in not enough contact time between the dyes and QKCF in the column and less diffusion of the dye into the pores of the QKCF (Vinodhini and Das 2010). At the end, the dyes might leave the column before equilibrium was reached. This phenomenon has been observed in other fixed-bed sorption systems (Rajeshkannan *et al.* 2013; Afroze *et al.* 2016).

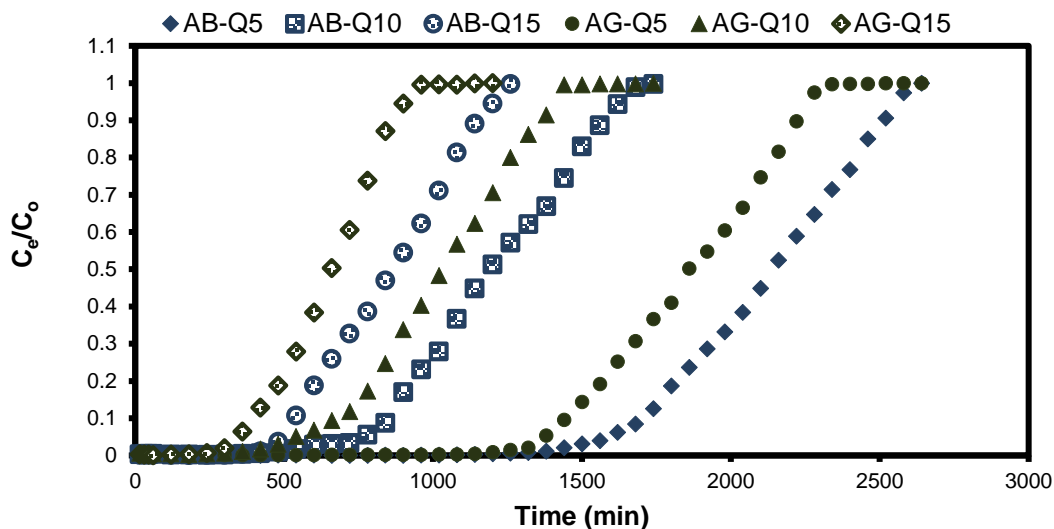


Fig. 11. Breakthrough curves for adsorption of AB and AG dyes in binary system for different flow rate (Q , mL/min) (100 mg/L of C_0 , bed depth of 6 cm, and a temperature of 27 ± 1 °C)

Table 3. Column Adsorption Data for AB and AG Dyes in Binary System onto QKCF

Dye in Binary System	Initial Dye Concentration (mg/L)	Bed Height (cm)	Flow Rate (mL/min)	Breakthrough Time t_b (min)	Complete Exhaustion Time t_e (min)	Bed Capacity at $t_{0.5}$ q_e (mg/g)
	20	6	10	3510	5520	120
	60	6	10	1420	2280	134
	100	6	10	770	1740	142
	100	4	10	460	1320	134
	100	8	10	1265	2280	156
	100	6	5	1590	2640	158
	100	6	15	490	1260	127
	20	6	10	3190	5160	109
	60	6	10	1265	2220	120
	100	6	10	535	1620	124
	100	4	10	350	1200	117
	100	8	10	1075	2160	132
	100	6	5	1375	2520	139
	100	6	15	400	1200	111

Column Dynamics Studies

The Thomas, Yoon-Nelson, and Bohart-Adams models were used to analyze the sorption performance of the anionic dyes through the column system.

Application of Thomas model

The data from experimental column studies were analyzed by the Thomas model. The Thomas hypothesis is based on an adsorption process that follows the Langmuir kinetics for the adsorption-desorption process. In this model it is presumed that no axial dispersion takes place for the adsorbate-adsorbent interactions. The model can be used

for the favorable or the unfavorable isotherms, and the linearized form for the model is given by Eq. 10 (Thomas 1944),

$$\ln\left(\frac{C_o}{C_t} - 1\right) = \frac{K_{TH} q_o m}{Q} - K_{TH} C_o t \quad (10)$$

where K_{TH} (mL/mg min) denotes the Thomas rate constant, the equilibrium adsorbate uptake is represented by q_o (mg/g), m (g) is the amount of the adsorbent present in the column, and the flow rate is denoted by Q (mL/min).

The rate constant (K_{TH}) and q_o (mg/g) were estimated from the linear plots of $\ln[(C_o/C_t)-1]$ against time, t (min). The estimated values of K_{TH} and q_o (mg/g) for the adsorption of AB and AG dyes in binary system are listed in Table 4.

The values of adsorption capacity, q_o (mg/g), increased with an increase in the initial dye concentration and bed depth. In contrast, q_o (mg/g) values decreased with an increase in the inlet dye flow rate. At a higher flow rate, the dye solution did not have enough time to diffuse into the whole QKCF adsorbent mass, resulting in a lower adsorption capacity. A similar trend was observed in the sorption of Brilliant Black dye onto chitosan beads impregnated with a cationic surfactant (Rouf and Nagapadma 2015).

Overall, the regression coefficient determined from the Thomas model indicated that the Thomas model could be used to predict adsorption performance for the adsorption of the AB and AG dyes in binary systems in a fixed-bed column.

Table 4. Thomas Model Parameters for AB and AG Dyes in Binary System at Different Conditions Using Linear Regression Analysis

Dye in Binary System	Initial Dye Concentration (mg/L)	Bed Height (cm)	Flow Rate (mL/min)	K_{TH} (mL/(min·mg))	q_o (mg/g)	R^2
	20	6	10	0.12	132.58	0.865
	60	6	10	0.143	143.13	0.879
	100	6	10	0.152	154.87	0.991
	100	4	10	0.16	151.574	0.989
	100	8	10	0.102	158.37	0.914
	100	6	5	0.082	162.72	0.929
	100	6	15	0.184	151.95	0.965
	20	6	10	0.13	121.33	0.903
	60	6	10	0.15	126.34	0.879
	100	6	10	0.158	130.05	0.993
	100	4	10	0.178	121.94	0.989
	100	8	10	0.104	135.5	0.918
	100	6	5	0.092	147.45	0.926
	100	6	15	0.224	126.58	0.988

Application of Yoon-Nelson model

A simple model was also developed by Yoon and Nelson (1984) for analyzing the column breakthrough performance. Decreasing the rate of the adsorption probability for each of the adsorbate particles is directly proportional to the likelihood of the adsorbate being adsorbed along with a likelihood of the occurrence of the adsorbate breakthrough taking place on the adsorbents (Baral *et al.* 2009). The linearized form for the Yoon-Nelson model is given by Eq. 11,

$$\ln\left(\frac{C_t}{C_0 - C_t}\right) = K_{YN}t - \tau K_{YN} \quad (11)$$

where K_{YN} (min^{-1}) refers to the rate constant and τ is the time needed for a 50% breakthrough of the adsorbate.

In the Yoon-Nelson model, the parameters K_{YN} and τ are estimated from the linear plots of $\ln(C_t/(C_0 - C_t))$ vs. $t(\text{min})$. The estimated parameters are listed in Table 5 for the adsorption of AB and AG dyes in the binary systems.

Overall, the experimental data fit well with Yoon-Nelson model and had a regression coefficient ranging from 0.865 to 0.993. Table 5 shows that the rate constant K_{YN} increased with increasing the initial dye concentration and flow rate for column dynamics of the adsorption of AB and AG dyes in the binary system. In this study, the time required for 50% exhaustion of column, τ (min), increased with an increase in bed height. Moreover, the value of τ (min) decreased with an increase in the initial concentration and flow rate.

Table 5. Yoon-Nelson Model Parameters for AB and AG Dyes in Binary System at Different Conditions using Linear Regression Analysis

Dye in Binary System	Initial Dye Concentration (mg/L)	Bed Height (cm)	Flow Rate (mL/min)	K_{YN} (min^{-1})	τ (min)	R^2
	20	6	10	0.0012	5568.5	0.865
	60	6	10	0.0043	2003.77	0.879
	100	6	10	0.0076	1300.92	0.991
	100	4	10	0.008	848.81	0.989
	100	8	10	0.0051	1773.75	0.914
	100	6	5	0.0041	2733.66	0.929
	100	6	15	0.0092	851.09	0.965
	20	6	10	0.0013	5095.85	0.903
	60	6	10	0.0045	1768.76	0.879
	100	6	10	0.0079	1092.41	0.993
	100	4	10	0.0089	682.85	0.989
	100	8	10	0.0052	1516.46	0.918
	100	6	5	0.0046	2477.17	0.926
	100	6	15	0.0112	708.87	0.988

Application of Adams-Bohart model

The breakthrough characteristics were further analyzed by using the Adams-Bohart model. This model is based on the surface reaction theory and predicts that the equilibrium is not instantaneous. Hence, the researchers stated that the adsorption rate was proportional to the residual adsorbent capacity and the adsorbate concentration (Goel *et al.* 2005). The mathematical equation of the Adams-Bohart model is given by Eq. 12,

$$\ln\left(\frac{C_t}{C_0}\right) = K_{AB}C_0t - \frac{K_{AB}N_0Z}{U_0} \quad (12)$$

where C_0 and C_t are the inlet and the outlet concentration of the dye molecules, respectively, Z (cm) is the height of the adsorbent bed, N_0 (mg/L) denotes the maximal dye uptake ability per unit volume of the adsorbent bed, the linear velocity is represented by U_0 (cm/min), and the mass transfer coefficient is denoted by K_{AB} (L/mg min).

When $\ln(C_t/C_0)$ values were plotted against time, $t(\text{min})$, the model constants, such as the mass transfer coefficient (K_{AB}) and maximum adsorption capacity (N_0), were determined from the slope and intercept of the curve. These values are shown in Table 6. A good correlation coefficient R^2 of more than 0.90 reflects that the model accurately describes the adsorption phenomenon of AB and AG dyes in a binary system.

Table 6. Adams-Bohart Model Parameters for AB and AG Dyes in Binary System at Different Conditions using Linear Regression Analysis

Dye in Binary System	Initial Dye Concentration (mg/L)	Bed Height (cm)	Flow Rate (mL/min)	K_{AB} (L/(mg·min))	N_0 (mg/L)	R^2
	20	6	10	0.00014	2181.17	0.923
	60	6	10	0.000123	2266.64	0.90
	100	6	10	0.000094	2424.59	0.958
	100	4	10	0.00011	2252.29	0.922
	100	8	10	0.000082	2619.69	0.908
	100	6	5	0.00007	2118.49	0.935
	100	6	15	0.000144	2608.81	.090
	20	6	10	0.00015	1958.99	0.964
	60	6	10	0.000123	2071.65	0.90
	100	6	10	0.000094	2124.82	0.952
	100	4	10	0.00012	2039.45	0.924
	100	8	10	0.000082	2273.67	0.920
	100	6	5	0.00008	1840.44	0.929
	100	6	15	0.000174	2321.58	0.932

CONCLUSIONS

1. Quaternized kenaf core fiber (QKCF) bead packed in a column exhibited very high capacity for adsorption of anionic dye. The maximum adsorption capacities for Acid Blue 25 (AB) and Acid Green 25 (AG) dyes from binary systems were 162.7 and 147.4 mg/g, respectively.
2. The advantages of QKCF are due to its minimum cost of processing by utilizing the abundant availability of kenaf core fiber (KCF) in tropical countries and reducing the cost of energy, as no thermal treatment was needed during processing.
3. Fixed bed column adsorption studies of binary acid dyes (AB and AG) onto QKCF were found to perform better with lower adsorbate inlet concentration (20 mg/L), lower feed flow rate (5 mL/min) and higher QKCF bed height (8 cm) for fixed-bed column.
4. The breakthrough curves were analyzed by using the Thomas model, Adams-Bohart model, and Yoon-Nelson model. The experimental data were in good agreement with theoretical results. This indicates that all models could be used to predict adsorption performance for the adsorption of the AB and AG dyes from binary systems in a fixed-bed column.

ACKNOWLEDGMENTS

The authors thank the Department of Chemical and Environmental Engineering and the engineering faculty of University Putra Malaysia for their facilities used throughout the research process. Furthermore, the authors acknowledge fiscal support from the ministry of higher education and scientific research in Iraq.

REFERENCES CITED

- Afroze, S., Kanti, T., and Ang, H. M. (2016). "Adsorption performance of continuous fixed-bed column for the removal of methylene blue (MB) dye using *Eucalyptus sheathiana* bark biomass," *Research on Chemical Intermediates* 42(3), 2343-2364.
- Ahmad, A. A., and Hameed, B. H. (2010). "Fixed-bed adsorption of reactive azo dye onto granular activated carbon prepared from waste," *Journal of Hazardous Materials* 175, 298-303. DOI: 10.1016/j.jhazmat.2009.10.003
- Ahmedna, M., Marshall, W. E., and Rao, R. M. (2000). "Production of granular activated carbons from select agricultural by-products and evaluation of their physical, chemical and adsorption properties," *Bioresource Technology* 71, 113-123. DOI: 10.1016/S0960-8524(99)00070-X
- Babel, S., and Kurniawan, T. A. (2003). "Low-cost adsorbents for heavy metals uptake from contaminated water: A review," *Journal of Hazardous Materials* B97, 219-243.
- Baral, S. S., Das, N., Ramulu, T. S., Sahoo, S. K., Das, S. N., and Chaudhury, G. R. (2009). "Removal of Cr (VI) by thermally activated weed *Salvinia cucullata* in a fixed-bed column," *Journal of Hazardous Materials* 161(2), 1427-1435. DOI:10.1016/j.jhazmat.2008.04.127
- Ekrami, E., and Okazi, M. (2010). "Analysis of dye concentration in binary dye solutions using derivative spectrophotometric techniques," *World Applied Science Journal* 11(8), 1025-1034.
- Goel, J., Kadirvelu, K., Rajagopal, C., and Carg, V. K. (2005). "Removal of lead(II) by adsorption using treated granular activated carbon: Batch and column studies," *Journal of Hazardous Materials* 125(1-3), 211-210. DOI: 10.1016/j.jhazmat.2005.05.032
- Hamdaoui, O. (2006). "Batch study of liquid-phase adsorption of methylene blue using cedar sawdust and crushed brick," *Journal of Hazardous Materials* 135(1-3), 264-273. DOI: 10.1016/j.jhazmat.2005.11.062
- Idan, I. J., Jamil, S. N. A., Abdullah, L. C., and Choong, T. S. Y. (2017). "Removal of reactive anionic dyes from binary solutions by adsorption onto quaternized kenaf core fiber," *International Journal of Chemical Engineering* (2017), Article ID 9792657. <https://doi.org/10.1155/2017/9792657>
- Indrani, J., Vasniwa, R., Shrivastava, D., and Jadhav, K. (2016). "Microorganism-based treatment of azo dyes," *Journal of Environmental Science and Technology* 9, 188-197. DOI: 10.3923/jest.2016.188.197
- Mondal, S. (2008). "Methods of dye removal from dye house effluent: An overview," *Environmental Engineering Science* 25(3), 383-396. <https://doi.org/10.1089/ees.2007.0049>
- Obaid, M. K., Abdullah, L. C., Mahdi, D. S., Idan, I. J., and Jamil, S. N. A. (2017). "Fixed-bed adsorption study for removing of reactive orange 16 and acid red 114

- dyes from aqueous solution using kenaf,” *International Journal of Research in Advanced Engineering and Technology* 3(1), 32-40.
- Rajeshkannan, R., Rajasimman, M., and Rajamohan, N. (2013). “Packed bed column studies for the removal of dyes using novel sorbent,” *Chemical Industry and Chemical Engineering Quarterly* 19(4), 461-470. DOI: 10.2298/CICEQ120407081R
- Pirsaheb, M., Shahmoradi, B., Khosravi, T., Karimi, K., and Zandsalimi, Y. (2016). “Solar degradation of malachite green using nickel-doped TiO₂ nanocatalysts,” *Desalination and Water Treatment* 57, 9881-9888. DOI: 10.1080/19443994.2015.1033764
- Rouf, S., and Nagapadma, M. (2015). “Modeling of fixed-bed column studies for adsorption of azo dye on chitosan impregnated with a cationic surfactant,” *International Journal of Scientific and Engineering Research* 6(2), 124-132.
- Tan, I. A. W., Ahmad, A. L., and Hameed, B. H. (2008). “Adsorption of basic dye using activated carbon prepared from oil palm shell: batch and fixed-bed studies,” *Desalination* 225(1-3), 13-28. DOI: 10.1016/j.desal.2007.07.005
- Thomas, H. C. (1944). “Heterogeneous Ion exchange in a flowing system,” *Journal of the American Chemical Society* 66(10), 1664-1666. DOI: 10.1021/ja01238a017
- Shahmoradi, B., Negahdary, M. and Maleki, A. (2012). “Hydrothermal synthesis of surface-modified, manganese-doped TiO₂ nanoparticles for photodegradation of methylene blue,” *Environmental Engineering Science* 29(11), 1032-1037. DOI: 10.1089/ees.2011.0519
- Shahmoradi, B., Maleki, A. and Byrappa, K. (2013). “Removal of Disperse Orange 25 using in situ surface-modified iron-doped TiO₂ nanoparticles,” *Desalination and Water Treatment* 53(13), 3615-3622. DOI: 10.1080/19443994.2013.873994
- Shivaraju, H. P., Midhun, G., Anil Kumar, K. M., Pallavi, S., Pallavi, N., and Shahmoradi, B. (2017). “Degradation of selected industrial dyes using Mg-doped TiO₂ polyscales under natural sun light as an alternative driving energy,” *Appl. Water Sci.*, 1-12. DOI 10.1007/s13201-017-0546-0
- Vinodhini, V., and Das, N. (2010). “Packed bed column studies on Cr(VI) removal from tannery waste water by neem sawdust,” *Desalination* 264, 9-14. DOI: 10.1016/j.desal.2010.06.073
- Yavari, S., Mahmodi, N. M., Teymouri, P., Shahmoradi, B., and Maleki, A. (2016). “Cobalt ferrite nanoparticles: Preparation, characterization and anionic dye removal capability,” *J. Taiwan Inst. Chem. Eng.* 59, 320-329. DOI: 10.1016/j.jtice.2015.08.011
- Yoon, Y. N., and Nelson, J. H. (1984). “Application of gas adsorption kinetics. Part I. A theoretical model of respirator cartridge service life,” *American Industrial Hygiene Association Journal* 45(8), 509-516.
- Zaini, N., and Khairul, S. N. K. (2014). “Adsorption of carbon dioxide on monoethanolamine (MEA)-impregnated kenaf core fiber by pressure swing adsorption system (PSA),” *Jurnal Teknologi (Sciences and Engineering)* 68(5), 11-16. DOI: 10.11113/jt.v68.3023

Article submitted: July 3, 2017; Peer review completed: September 17, 2017; Revised version received: October 2, 2017; Accepted: October 4, 2017; Published: October 9, 2017.

DOI: 10.15376/biores.12.4.8870-8885